Energy & Environmental Science

Structural regulation-induced Li-electron disentanglement for stabilized oxygen redox of Li-excess disordered rock-salt cathode materials

Journal:	*Energy & Environmental Science*
Manuscript ID	EE-COM-02-2024-000638.R1
Article Type:	Communication
Date Submitted by the Author:	03-Jun-2024
Complete List of Authors:	Jiao, Sichen; Institute of Physics, Chinese Academy of Sciences, Renewable Energy Sun, Yujian; Institute of Physics, Chinese Academy of Sciences, Renewable Energy Shi, Dekai; Institute of Physics, Chinese Academy of Sciences, Renewable Energy Zhang, Yuanpeng; Oak Ridge National Laboratory Wang, Xuelong; Institute of Physics, Chinese Academy of Sciences, Renewable Energy Liu, Jue; Oak Ridge National Laboratory, Chemical and engineering Materials Kang, Le; Institute of High Energy Physics Chinese Academy of Sciences Wang, Fangwei; Institute of Physics, Chinese Academy of Sciences Yu, Xiqian; Institute of Physics, Chinese Academy of Sciences, Renewable Energy; Brookhaven National Laboratory, Chemistry Li, Hong; Institute of Physics, Chinese Academy of Sciences, Chen, Liquan; The Institute of Physics, Chinese Academy of Sciences, Huang, Xuejie; Institute of Physics(CAS),

Structural regulation-induced Li-electron disentanglement for stabilized oxygen redox of Li-excess disordered rock-salt cathode materials

Sichen Jiao[#], Yujian Sun[#], Dekai Shi, Yuanpeng Zhang, Xuelong Wang[*], Jue Liu[*], Le Kang, Fangwei Wang, Xiqian Yu[*], Hong Li, Liquan Chen, and Xuejie Huang

Data availability statements

Data are available upon reasonable request from the authors

Broader Context:

Rationally harnessing extra capacity from oxygen redox while achieving long-cycling stability has long been sought after in the research of cathode materials for lithium-ion batteries. Highly active oxidized oxygen anions after Li extraction are prone to migrate, pair, and eventually get lost, which leads to structural deterioration and irreversible capacity loss. Disordered rock-salt cathode material with multiple cation species provides a lattice for various oxygen environments to coexist. Regulating the arrangements of different cations could tune the charge compensation from oxygen redox in different environment and possibly stabilize the oxidized oxygen anions in certain coordination shell. Here, with modified cation distribution induced by fluorination, we reveal and demonstrate the beneficial effects of spatially disentangled Li extraction and electron depletion on the cycling performance of DRX cathode. In this regard, enhanced cycling stability can be achieved in an intentionally designed DRX oxide composition by us taking advantages of the Li-electron disentanglement effects enabled by local structure manipulation.

COMMUNICATION

Structural regulation-induced Li-electron disentanglement for stabilized oxygen redox of Li-excess disordered rock-salt cathode materials

Received 00th January 20xx,
Accepted 00th January 20xx

DOI: 10.1039/x0xx00000x

Sichen Jiao,‡[ab] Yujian Sun,‡[ab] Dekai Shi,[ab] Yuanpeng Zhang,[c] Xuelong Wang,*[a] Jue Liu,*[c] Le Kang,[d] Fangwei Wang,[b] Xiqian Yu,*[ab] Hong Li,[ab] Liquan Chen[a] and Xuejie Huang[a]

Since the discovery of its electrochemical activity, Li-excess disordered rock-salt (DRX) cathode material has received worldwide attention as it sets up a new way to exploit oxygen redox beyond the conventional layered structure with late-3d transition metal. However, the intricate structure-function relationship in the disordered lattice of DRX material fogs up the researcher's lens on the underlying redox mechanisms. In this study, we employ a synergistic approach combining neutron total scattering with reverse Monte Carlo modeling and density functional theory calculations to unravel the landscape of oxygen redox reactions in DRX. Redox activities are evaluated in diverse oxygen clusters (OLi_xTM_{6-x}) and the spatial distribution of these clusters in the model DRX structure ($Li_{1.16}Ti_{0.37}Ni_{0.37}Nb_{0.1}O_2$ and $Li_{1.2}Ti_{0.35}Ni_{0.35}Nb_{0.1}O_{1.8}F_{0.2}$) is explicitly counted. Results unveil that through regulating the short-range ordering between cations, flourine atoms can effectively decouple the location of Li extraction and electron depletion. Such disentanglement between the Li reservoir and electron reservoir in the DRX lattice could play a pivotal role in protecting the oxidized oxygen and preserving the lattice framework during cycling. Through a tentatively designed non-fluorinated DRX oxide realizing similar Li-electron decoupling, an obvious enhancement of cycling capability can be achieved without compromising the capacity release.

Amid the transition from fossil fuel to sustainable energy sources, the demand for high-performance lithium-ion batteries (LIBs) is more intense than ever.[1] Material innovation has always been the major driving force for LIB technology advancement.[2,3,4] The discovery of Li-excess disordered rock-salt (DRX) material being electrochemical active sets a great example of this paradigm.[5,6] First brought to attention by Ceder et al., DRX materials are constantly under scrutiny as they free the cathode material design from the constraint of layered structure and late-3d transition metal (TM) elements.[7] The source of unexpected Li capacity released from DRX material is delicately explained by the proposed percolation theory. Our recent works successfully extended and applied this theory to reveal the effects of d^0 TM cation displacement and how fluorine substitution can reorganize the percolation network across different scales.[8,9]

Capacity-wise, DRX materials have been understood thoroughly, yet redox-wise they have not. Questions such as how TM/O redox takes action and what their proportions are in the measured capacity have not been tackled much.[10] The cause of this plight is rooted in the structural complexity of DRX material where Li and TM sites are mixed up in various types of short-range ordering (SRO). Problems are challenging, yet many excellent works have managed to reveal different important mechanisms behind the redox behavior in Li-excess cathode materials. For example, Tarascon et al. uncovered that certain coordinated TM-O couples can act as redox centers where O oxidation could proceed through regenerating the mediator TM cation and cause resultant peroxo-like O pairs.[11] Ceder et al. revealed that linear Li-O-Li configuration can cause increasing O 2p electronic states near the Fermi level and activate O redox.[12] Xia et al. further disclosed that second shell cation species can also affect the center TM-O couple's redox by thermodynamically activating the charge transfer process from O to TMs.[13] Recently, Yabuuchi et al. found that structural disorder may be beneficial for activating O redox through the formation of linear Ni-O-Ni configuration to stabilize oxidized O.[14] All these previous studies pointed out the tight relationship between local structure and redox behavior.[15,16,17]

[a] Beijing Frontier Research Center on Clean Energy, Institute of Physics, Chinese Academy of Sciences, Beijing 100190, China. Email: xyu@iphy.ac.cn; wangxuelong@iphy.ac.cn
[b] Center of Materials Science and Optoelectronics Engineering, University of Chinese Academy of Sciences, Beijing 100049, China.
[c] Neutron Scattering Division, Oak Ridge National Laboratory, Oak Ridge, TN 37831, USA. Email: liuj1@ornl.gov
[d] Institute of High Energy Physics, Chinese Academy of Sciences, Beijing 100049, China; Spallation Neutron Source Science Centre, Dongguan 523803, China.
† Electronic Supplementary Information (ESI) available. See DOI: 10.1039/x0xx00000x
‡ These authors contributed equally.

DRX materials have a rich amount of local structure type compared to layer cathode materials.[18] It would be of high scientific interest and application relevance to tune the redox behavior of DRX materials by manipulating the distribution of different local structures. Several mechanisms may take effect at the same time and optimal performance could be achieved benefitting from different mechanisms.

Technically, spectroscopic techniques including X-ray photoemission spectroscopy (XPS), X-ray absorption spectroscopy (XAS), and resonant inelastic X-ray scattering (RIXS) have been extensively employed to discern the capacity contribution from oxygen oxidation in cathode materials.[19] The relatively uniform oxygen environment in conventional oxide cathodes facilitates the establishment of the correlation between measured average oxygen redox contribution with bulk structure evolution. However, the diverse local structural features in DRX material obstruct discerning the site-specific redox behaviour with bulk-averaged spectroscopic results. Though techniques focusing on localized features such as transmission electron microscopy (TEM) and nuclear magnetic resonance spectroscopy (NMR) can characterize the structure and redox of a specific cluster, obtaining statistically reliable results with them is extremely exhausting.[8] In current work, a combination of multiscale structural characterization and theoretical calculations offers a potential solution for studying site-specific oxygen redox reactions in DRX materials.

Here, we quantitatively show how local structure configuration and their distribution (i.e., SRO) are related to the active redox contribution. Following the uncovered trend, we substantially enhanced the cycling stability without sacrificing the capacity in a tentatively designed DRX material. Moreover, we propose the critical role of spatial decoupling between Li^+ and electron reservoir in stabilizing the oxidized O^{2-} and exploiting the extra capacity from oxygen redox. The recognized effect can be generalized to future designs of high-energy-density and long cycle-life oxygen redox-active cathode materials.

As depicted in the middle panel of Fig. 1a, the combined utilization of neutron pair distribution function (PDF) measurement and reverse Monte Carlo (RMC) modelling enables recovering multiscale structural features of DRX material. The experimental technical details and basic morphological and structural information related to the DRX material samples presented here can be found in the supporting information (SI) and our previous works.[8,9] After obtaining the PDF patterns in the experiment, the pivotal step is the reconstruction of the DRX material lattice in a supersized cell (~10 nm in each axis) with which the 3D percolation network for

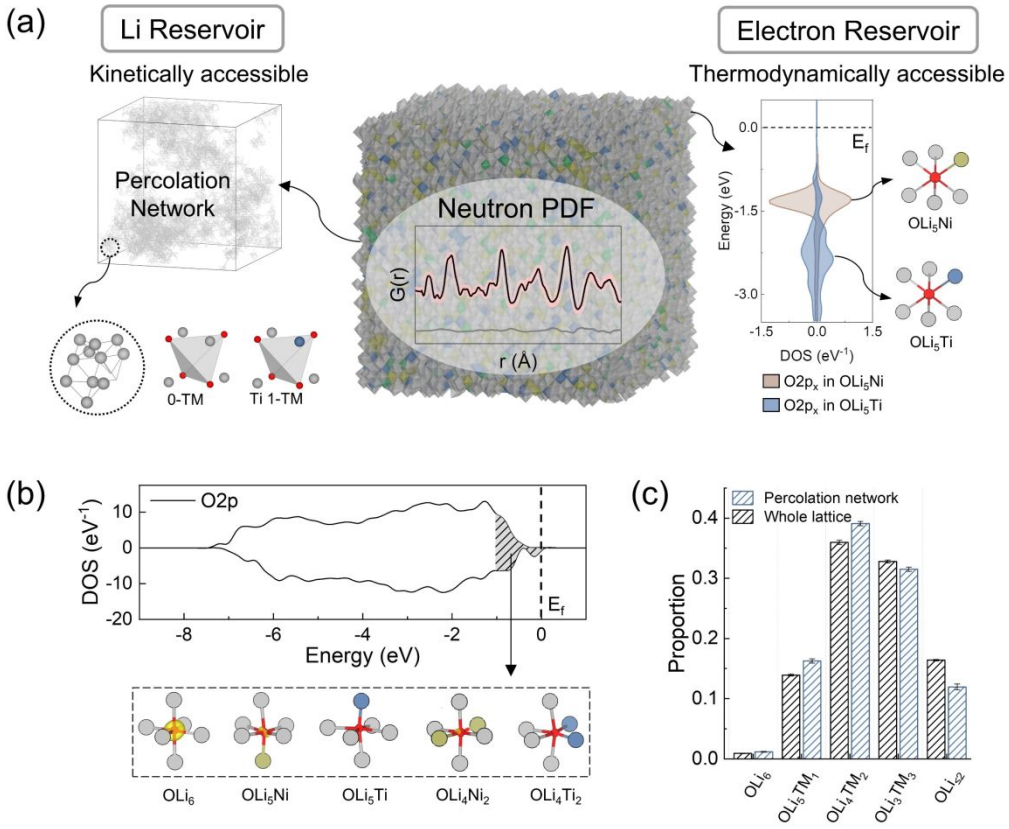

Fig. 1 (a) Overview on the source of lithium atom (percolation network) and electron (calculated pDOS) in DRX, where the DRX supercell can be reconstructed through the combination of neutron PDF measurements and RMC modeling. (b) Calculated overall O 2p pDOS of LTNNO, with the bottom panel displaying the isosurface plot of charge density around oxygen atoms within specific OLi_xTM_{6-x} clusters, in the energy range of -1.0 to 0 eV (the shaded region in the pDOS). (c) The comparison between the proportion of different oxygen clusters within the whole lattice and percolation network in LTNNO. All the results are statistically counted among five independent RMC runs.

Li^+ transportation and statistics on local structures can be

obtained. The percolating theory of DRX material refers to that accessible Li^+ are those interconnected through fast hopping channels (0TM channels through tetrahedral sites facing no TM atoms, and partial 1TM channels through tetrahedral sites where TM neighbor displaces far enough).[7,8] Therefore, the percolation network depicts where the Li^+ reservoir is and dictates the largest Li capacity that can be released from DRX material (left panel of Fig. 1a). As for the electron source during extraction of Li^+, the physical picture is still vague. Electronic band structure calculation, displayed as the partial density of states (pDOS), in the right panel of Fig. 1a shows the energetic order for electronic states of different local clusters. Thermodynamically, the closer an electronic state is to the Fermi level, the more likely electronic depletion happens to this state during Li extraction. However, the DOS spectrum only suggests the energetic distribution of different electronic states. The spatial distribution of electronic states corresponding to active redox hasn't been explicit yet. In conventional layered structure material, the ordered arrangement of the Li layer/TM layer would lead to the natural assumption that electronic depletion happens in the TM layer next to the Li layer where delithiation occurs. More specifically, electrons should be extracted from the TM and O atoms in the closest shell to the extracted Li atom. Such presumption is indeed usually true for layered structure cathode materials. However, since in DRX material Li and TM sites are completely mixed and multiple TM elements are somewhat randomly distributed over a lattice framework, the prior assumption may not be applicable anymore. In fact, as we will show later, the location of the electron source cannot be taken for granted so willingly.

To unveil the spatial distribution of electron sources corresponding to different redox reactions in the DRX system, a model material $Li_{1.16}Ti_{0.37}Ni_{0.37}Nb_{0.1}O_2$ (LTNNO) is chosen in the current study where both TM and O redox were proven to be active. Density functional theory (DFT) calculations were employed to correlate electronic states with certain structural features. Further details on the DFT calculation (Note 1 in SI) and workflow (Fig. S1) are available in SI. Upon examining the atomic charge and magnetization evolution during delithiation (Fig. S2-5), it can be inferred that charge compensation occurs through the initial oxidation of Ni atoms, and is succeeded by the oxidation of oxygen atoms at high voltages. The occurrence of TM redox and oxygen redox aligns with previous experimental findings.[20] The disordered nature of DRX is expected to broaden the oxygen 2p band due to various coordinating environments around oxygen atoms, specifically, octahedral cluster OLi_xTM_{6-x} in the close-packed cubic lattice (for LTNNO, TM=Ti/Ni/Nb, x=0, 1, 2, 3, 4, 5, 6). The calculated overall O 2p pDOS is shown in Fig. 1b. As the oxygen redox reaction is closely related to the non-bonding linear Li-O-Li configuration, the O 2p pDOS along the Li-O-Li direction in each OLi_xTM_{6-x} type is calculated separately as well. When fully lithiated, substantial differences in peak position and O 2p pDOS profile were observed (Fig. S6 and S7) among different clusters. Overall, the number of lithium atoms and TM types are the major factors affecting the pDOS feature. This can be further confirmed by visualizing the electron clouds originating from the Li-O-Li configuration around the active oxygen atoms. As displayed in the bottom panel of Fig. 1b, in the energy range just below the Fermi level (-1.0 to 0 eV vs. E_f), the electron density is predominantly associated with the OLi_6 cluster and partly contributed by the OLi_5Ni cluster. Electron clouds associated with other oxygen clusters only begin to emerge at deeper energy levels (Fig. S8). Consistent with our results, previous theoretical studies have also noted that the so-called non-bonding oxygen state can be energetically modulated by neighbouring TM species.[21,22] Thus, the number and types of TM atoms within the OLi_xTM_{6-x} clusters can significantly influence the energy level of the redox-active O 2p states in DRX materials.

Regarding the lithium number in coordination, the more lithium atoms appear in the first coordinating shell, the closer non-bonding O states move toward the Fermi level, indicating more active oxygen redox in the Li-rich cluster. Based on this, we could roughly classify different OLi_xTM_{6-x} clusters into two kinds, namely Li-rich ($x \geqslant 4$) and Li-poor ($x \leqslant 3$). In the Li-rich cluster, oxygen redox is more prone to be activated while TM-only redox is more likely to happen in the Li-poor cluster. Besides redox preference being different, fast Li migration channels are more likely to occur around the Li-rich cluster than the Li-poor cluster. Therefore, Li-rich clusters may take higher fractions in the percolation network, which establishes the foundation for correlating the spatial distribution of the Li reservoir with the electron reservoir. Specific statistics on cluster counts within the RMC-fitted supercell reveal a dominant presence of OLi_4TM_2 and OLi_3TM_3 within the whole lattice framework, amounting to 36.0% and 32.8%, respectively (illustrated by the black columns in Fig.1c). Meanwhile in the percolation network, the proportion of Li-rich clusters increases to 56.5% (vs. 50.8% in the whole lattice), consistent with the presumption. Since lithium atoms would be extracted from the percolation network during charging, prevailing Li-rich clusters in the network may facilitate high oxygen redox participation in the charge compensation.

However, TM species in the OLi_xTM_{6-x} cluster also strongly affect the energy level of O states. At a given number of coordinating lithium atoms, such as x=5 (OLi_5TM, right panel of Fig. 1a), the d^0 nature of the Ti element effectively shifts the non-bonding state to a deeper energy level compared to the Ni element. The distinct oxygen redox activity is further checked by examining the alteration in electronic structure after delithiation. Fig. S9 compares the pDOS of O 2p orbitals in two typical oxygen environments, OLi_4TiNi and OLi_4Ti_2. After delithiation, a notable increase of empty O 2p states above the Fermi level occurs in the OLi_4TiNi environment compared to OLi_4Ti_2, suggesting that the charge compensation is mainly from oxidized oxygen atoms. Therefore, a more detailed analysis of OLi_xTM_{6-x} clusters with different TM species is needed to break down the charge contribution from different redoxes and locate the electronic reservoir. We chose atomic magnetic moment change after delithiation as an indicator for oxidation state change since it has been proven to have high sensitivity, especially in reflecting the electron configuration evolution

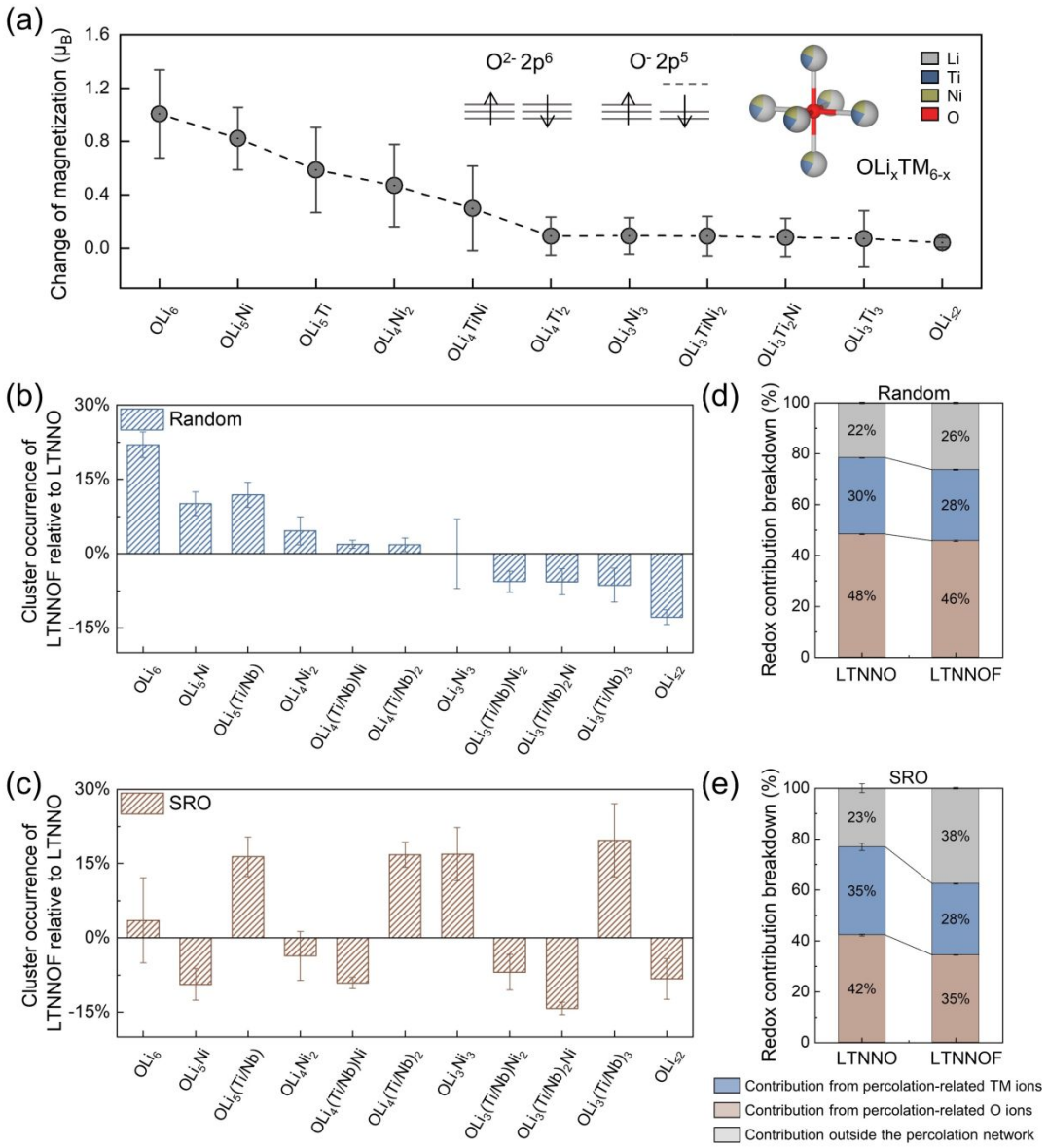

Fig. 2 (a) Changes in atomic magnetization upon delithiation of various oxygen atom types, with results statistically averaged among twelve structures for DFT calculation. Occurrences of oxygen clusters involved in the percolation network of LTNNOF relative to LTNNO in the case of (b) a hypothetical structure with cations randomly distributed and (c) a realistic structure with SRO derived from nPDF results and RMC modeling. All the results are statistically counted among five independent RMC runs. Redox contribution breakdown comparison between LTNNO and LTNNOF in the case of (d) random and (e) SRO.

from $2p^6$ to $2p^{6-x}$ for O.[12] The calculated results are summarized in Fig. 2a and a larger deviation from zero means a more oxidized oxygen atom. In line with the pDOS analysis (Fig.1), oxygen atoms in a Li-poor environment (OLi_xTM_{6-x}, $x \leqslant 3$) show almost no change in magnetization. More importantly, environments with Ti/Nb abundance exhibit suppressed oxygen oxidation, which suggests enriched Ti/Nb involvement in the percolation network may lower the O redox contribution to the capacity.

The involvement of Li-rich and Ti/Nb abundant clusters in the percolation network have seemingly opposite effects on tuning O redox participation, which leaves room for altering the redox proportion through manipulating the cluster distribution. Following this thought, we conducted a thorough comparison between LTNNO and its fluorinated counterpart $Li_{1.2}Ti_{0.35}Ni_{0.35}Nb_{0.1}O_{1.8}F_{0.2}$ (LTNNOF) to investigate how the arrangement of the diverse oxygen environments affects the contribution to capacity from the oxygen redox reactions in DRX. Their lab-based characterizations, including composition, structure, and morphology, have been reported before.[9] The F-induced atomic-scale alterations on the second-nearest oxygen atoms were subtle and related discussions can be found in SI (Note 2 and Fig. S10-12). Our recent work unveiled that fluorination could effectively reorganize the spatial arrangement of cations in LTNNO across different length scales from the atomic level to short-range scale and eventually global structure.[9] Therefore, detailed statistics of these cluster distributions can help clarify their correlation with redox

proportion. Considering the percolation network is the actual location where Li extraction happens, hereafter we attribute the TM/O ions bonded with percolating lithium ions to the term "percolation-related" TM/O ions. Details about the statistical analysis can be found in Note 3 in SI. The spatial distribution of the lithium percolation network and percolation-related TM/O ions are visualized in the LTNNO RMC supercell (Fig. S13).

Statistical analysis on the proportion of different OLi_xTM_{6-x} clusters involved in the percolation network is shown in Fig. 2b-c. To demonstrate the influence of SRO, we also listed the results of the randomly distributed cations for comparison. Each column represents the cluster occurrence difference between LTNNOF and LTNNO in percentage and the error bar shows the standard deviation among five independent RMC runs. Due to the minimal amount of Nb and similar d^0 character, Ti and Nb atoms are not differentiated here. In a fully random structure, the incorporation of the F atom leads to an increase in the Li-rich environment ($x \geqslant 4$) and a decrease in the Li-poor ones ($x \leqslant 3$). This nearly monotonic trend can be rationalized by the changes in nominal composition. When cations are randomly distributed, the occurrence probability of the OLi_xTM_{6-x} cluster is simply determined by the cation concentration and not related to anion species. Higher lithium content in LTNNOF ($Li_{1.2}$ in LTNNOF vs. $Li_{1.16}$ in LTNNO) would promote the occurrence of clusters containing more Li atoms. In contrast, when realistic SRO is imposed, results change completely (Fig. 2c). Specifically, the proportions of Li-rich Ni-containing clusters including OLi_5Ni, OLi_4Ni_2, and OLi_4(Ti/Nb)Ni are diminishing after fluorination, while Ti/Nb abundant clusters including OLi_5(Ti/Nb), $OLi_4(Ti/Nb)_2$, and $OLi_3(Ti/Nb)_3$ are appearing much

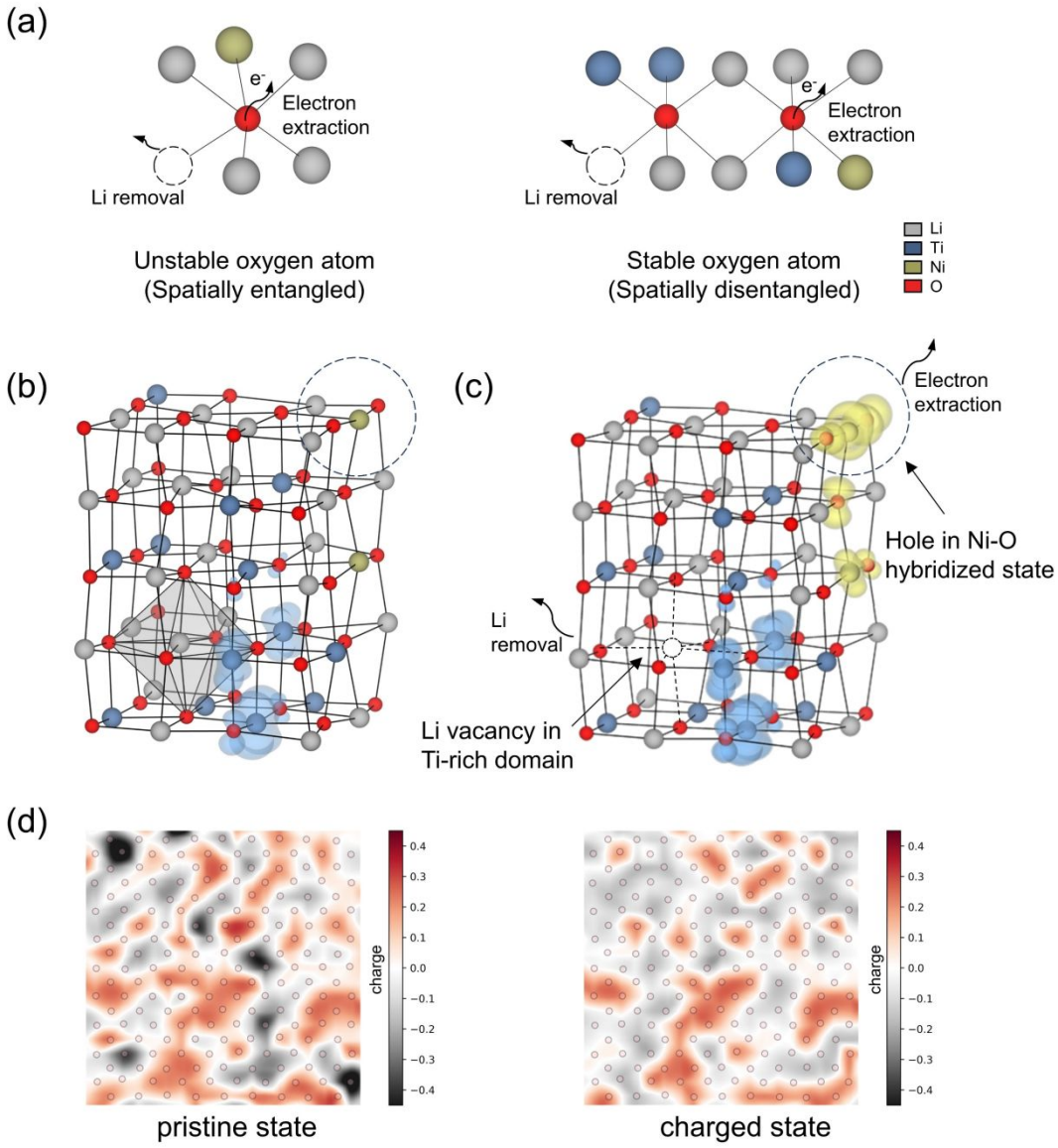

Fig. 3 (a) Schematic illustration of unstable oxidized oxygen atoms and stable ones. Iso-surface of the hole density within the Ti-rich domain at (b) pristine state and (c) delithiated state in the energy range of 0 to 0.4 eV above Fermi level, where yellow is used to highlight the newly emerged states. (d) The two-dimensional Bader charge distribution of oxygen clusters at the pristine state and charged state of LTNNO (depicted in one arbitrarily selected (100) crystal plane of the LTNNO supercell).

more. This trend is consistent with our previous findings where Li^{+}-Ti^{4+} have preferential coordination.[9] Fluorine's attraction to Li^{+} results in Li-Ti rich region and exclusion of Ni^{2+} from the coordination shell around Li. As a side effect, the Ni-O subdomain begins to emerge after fluorination which is responsible for the increasing occurrence of the OLi_3Ni_3 cluster.

Combining the evaluation of oxygen oxidation in different clusters after delithiation (Fig. 2a) with the statistics on each type cluster's appearance (Fig. 2b-c), we are now able to conduct a quantitative breakdown of the redox contribution (Fig. 2d-e, details in Note 4 of SI) (percolation-related TM cations, percolation-related O anions, and outside the percolation network). Fluorination of DRX oxide has been commonly believed to suppress O redox and promote TM redox due to the lowered valence state of TM cations.[23] Current results disclose much more details behind this oversimplified understanding. 1) Comparatively speaking between LTNNO and LTNNOF, cation arrangement being either random or SRO, contributions from both percolation-related O and TM redox decrease upon fluorination. In the fully random case (Fig. 2d), the decrement is little (~2%) which is simply a consequence of more Ti/Nb abundant clusters occurrence than Ni-containing ones due to lower Ni content and higher Li content in LTNNOF. When taking SRO into account (Fig. 2e), the decrement of percolation-related redox after fluorination becomes more significant (~7%), which could be attributed to the promoted Ti/Nb cluster occurrence and diminished Ni cluster occurrence in the percolation network. The inactive nature of Ti/Nb cation and suppressed O redox in a Ti/Nb abundant environment amount to this result. 2) Comparatively speaking between random case and SRO case, the effect of SRO on redox contribution is vastly different between LTNNO and LTNNOF. In pure oxide, SRO only affects the relative proportion between percolation-related TM and O contribution (30% to 35% for TM, 48% to 42% for O). This is because correlations between cation species lower the probability of Li-rich cluster occurrence in the percolation network leaving some Li-rich domains isolated. In LTNNOF, SRO only affects the relative proportion between percolation-related O contribution and contribution outside of the percolation network (46% to 35% for O, 26% to 38% for outside). This can be rationalized by the much more promoted Ti/Nb appearance in the percolation-related clusters, especially the Li-rich ones. The inactive Ti/Nb cation and low activity of O in Ti/Nb-containing clusters lead to the much-lowered contribution from percolation-related O with SRO. Nevertheless, instead of raising percolation-related TM contribution to balance, F-induced SRO results in a large contribution from outside the percolation network. This finding is of high interest since it suggests electron depletion prefers to occur outside of the percolation network of the fluorinated DRX material, i.e., the electron reservoir is spatially detached from the Li reservoir.

The extraction of lithium atoms is concomitant with the oxidation of adjacent atoms in conventional layered oxide cathode materials, especially in the Ni/Mn-based oxide material, signifying that Li vacancy and electrons deficient center are spatially entangled (left panel of Fig. 3a).[24] In a Li-rich local configuration around O^{2-}, such entanglement means a high possibility of structural degradation after Li removal since oxidized oxygen anions can easily migrate to Li vacancy and get lost.[25,26] In contrast, the right panel in Fig. 3a illustrates an intriguing scenario of disentanglement. The spatially decoupled lithium vacancy and electron-hole may offer a new way to stabilize the oxidized O anion since the electron-depleted oxygen atoms are still fully coordinated. With this insight, one can envisage a simultaneous achievement of extra capacity from oxygen redox and stabilized oxygen framework. To examine the possible existence of such scenario, the change of charge density's spatial distribution upon Li extraction was evaluated in a regularly-sized DRX cell (see more details in Fig. S14-15). An octahedrally coordinated lithium atom in the Ti-rich domain (grey region in Fig. 3b) was intentionally extracted (Fig. 3c). Conspicuously, new holes are generated around the Ni atom situated 7.86 Å away from the lithium vacancy, a notable departure from its pristine state. A closer inspection reveals that the electron depletion happens to the σ-type hybridized state between the Ni eg state and the O 2p state. To compensate for the negatively charged lithium vacancy, electron loss occurs in a cluster outside the Ti-rich domain instead of vicinity. It should be noted that the calculation here only describes the electronic structure at the thermodynamic ground state. The detailed kinetic process of extracting lithium and electrons might involve complicated intermediate states. Mechanisms similar to previously proposed ones [27,28] may all take effect here, which is beyond the scope of current work.

One might argue that spatially coupled Li and electron extraction are necessary for maintaining charge neutrality. In layered oxide cathodes, the local environment around oxygen atoms only presents as OLi_3TM_3 (TM^{+3}, e.g., $LiCoO_2$,) and OLi_4TM_2 (TM^{+4}, e.g., Li_2MnO_3), where local charge neutrality can be naturally achieved within a single octahedral cluster. In DRX material, diverse oxygen environments coexist and charge distribution is highly non-uniform. Fig. 3d displays charge density distribution, where the magnitude of oxygen clusters' charge is superimposed on a (100) plane of LTNNO (see more details in Fig. S16). Upon delithiation, different types of oxygen clusters exhibit varying extents of charge transfer, and the overall lattice tends to become charge-neutral. In other words, the charge of the system is intricately balanced among different clusters on a broader scale, rather than within the single cluster.

The proposed spatial decoupling between Li and electron reservoir and their separated extraction has a profound influence on the performance of the DRX cathode. As previous studies pointed out, oxygen redox activation is very likely responsible for the poor cycling capability of DRX material.[18,29] Oxygen redox taking place outside the percolation network maintains the full coordination environment around oxidized oxygen, potentially enhancing the O redox reversibility and structural integrity after high voltage charging. The enhanced cycling stability of LTNNOF compared with LTNNO verifies this presumption to some extent. As illustrated in Fig. 4a. LTNNO cathode only shows a capacity retention of 68% after 30 cycles, while it increases to 89% in LTNNOF which could be attributed to the much-increased redox contribution outside of the

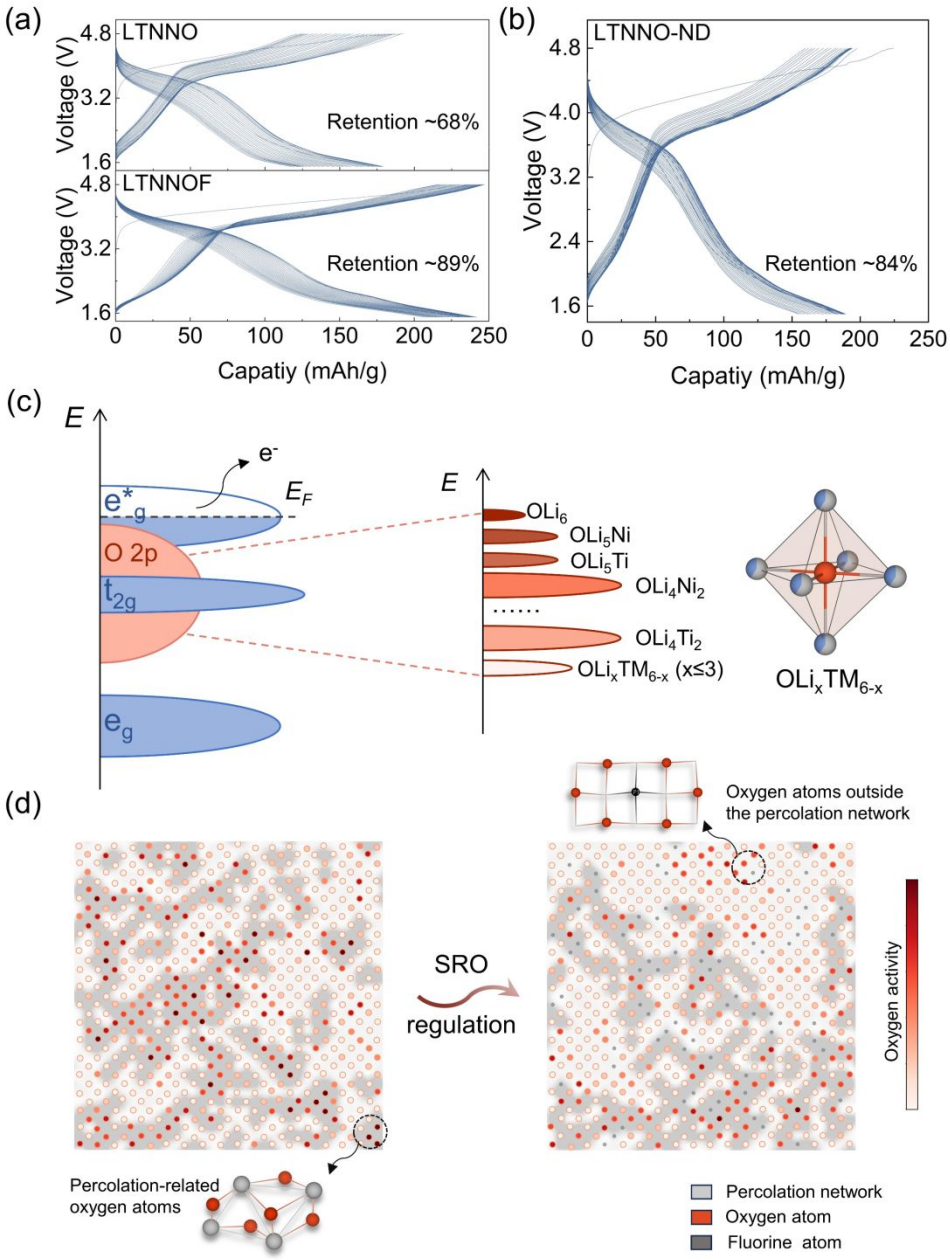

Fig. 4 (a) Room-temperature cycling performance of (a) LTNNO, LTNNOF, and (b) LTNNO-ND between the voltages of 1.5-4.8V at 50 mA/g during 30 cycles. (c) Illustrative energy band diagram for DRX cathode material, where the O 2p band is significantly broadened due to diverse oxygen environments (OLi_xTM_{6-x}). (d) Schematic illustration of how SRO rearranges the oxygen atom distribution in the DRX cathode material. The 2D representation is depicted on a (100) crystal plane, featuring the region of percolation network (shaded area), oxygen sites (circle in varying red), and fluorine sites (dark grey dot). Different shades of red indicate different activity levels of O atoms, the darker the higher activity. On left, majority of percolation-related O atoms have high activity. On right after SRO regulation, the amount of percolation-related active O atoms becomes much less, while many O atoms of high activity appear outside the percolation network.

percolation network. However, since fluorination indeed lowers the TM valence state, the beneficial effects on cycling from overall larger TM redox contribution cannot be excluded. Therefore, as a proof of concept, a fluorine-free oxide derivative of LTNNO was intentionally synthesized with a 5% reduction of Ni content ($Li_{1.2}Ti_{0.36}Ni_{0.33}Nb_{0.11}O_2$, LTNNO-ND where ND means Ni-deficiency) (XRD pattern in Fig. S17). LTNNO-ND exhibits a higher average valence state of Ni (~+2.45) compared to LTNNO (~+2.32), which in conventional belief means a higher level of O redox participation and potentially poorer cycling performance. Surprisingly, LTNNO-ND demonstrates a much-improved cycling stability with a capacity retention of 84% after 30 cycles (Fig. 4b) and a slightly higher level of capacity release (189 mAh/g) compared to LTNNO (179 mAh/g). This contradiction further underscores the necessity of understanding multiscale structural response to compositional change in DRX materials beyond the analysis of elemental chemical states. The unexpected results can be easily explained by the newly proposed mechanism. The elevated nominal valence state of Ni atoms would repel Ti^{4+} as neighbor due to raised electrostatic

repulsion. Meanwhile higher Li content would cause a higher proportion of Li-rich Ti-abundant clusters through which a percolation network can easily form. Consequently, the Li reservoir is filled with electronically inert Li/Ti-rich clusters while the electron reservoir consisting mostly of Ni-containing clusters is spatially detached. Even though oxygen redox may still participate in charge compensation, it very likely happens outside the percolation network, and the oxidized oxygen anions are well protected.

The disordered nature of DRX material introduces oxygen atoms to a diverse coordinating environment, denoted as OLi_xTM_{6-x}. Thermodynamically, the O 2p band undergoes significant broadening across a wide energy range due to this diversity (Fig. 4c). The redox activity of each oxygen atom is determined by both the quantity of lithium atoms and the type of TM species in coordination. On a broader length scale, the spatial arrangement of distinct oxygen types, depending largely on SRO, critically influences oxygen redox reactions within the DRX material. When oxygen atoms with high redox activity are bonded to percolating lithium atoms, Li extraction around the electron-depleted O would easily cause oxygen loss and structural deterioration (left panel of Fig. 4d). However, if SRO is regulated through some strategy such as fluorination so that Li reservoir is spatially detached from electron reservoir, the oxidized oxygen atoms are then well protected by the intact coordination shell outside the percolation network (right panel of Fig. 4d).

Very recently, Outka et al. revealed a pronounced electron localization effect in Ni-based DRX materials through well-designed experiments.[30] Their resonance Raman spectroscopy provided compelling evidence that electron hopping is restricted to a network of NiO_6 octahedra, dispersed within a matrix of insulating d^0-TMO_6 octahedra, such as TiO_6. Similarly, Lee et al. theoretically identified a distinctive electron percolation network comprising edge-shared and corner-shared MnO_6 octahedra in Mn-DRX.[31] Collectively, these findings, alongside our present results, strongly indicate that the Li and electron percolation networks in DRX materials can be effectively decoupled. For DRX materials with the general formula $Li_{1+X}TM_yTM''_{1-x-y}O_2$ (where TM and TM'' denote redox-active and -inactive transition metal elements, respectively), four types of oxygen clusters with varying capabilities to conduct Li^+ and e^- can be distinguished, as schematically depicted in Fig. S18. DRX materials can be conceptualized as complex composites of Li^+-conducting motifs (Li-rich and TM/TM''-containing clusters) and e^--conducting motifs (Li-rich/poor TM-containing clusters). The exceptional structural flexibility of DRX materials offers substantial opportunities to manipulate the number and arrangement of these clusters, thereby enabling Li-electron disentanglement to stabilize oxygen redox, as demonstrated herein. Moreover, we propose that this structural regulation strategy can be extended to conventional layered Li-rich cathodes, where the extent and type of in-plane disorder within the Li/TM plane can be controlled. Overall, the novel structure-redox interactions identified in DRX materials not only pave the way for advanced manipulation of oxygen redox behavior in DRX but also inspire the rational design of high-capacity, long- cycling Li/Na oxide cathode materials by controlling structural disorder.

Methods

Material synthesis:

The LTNNO and LTNNOF cathode materials were prepared via a straightforward solid-state sintering method, as detailed in our previous publication.[9,32] Synthesis of the LTNNO-ND cathode material followed a similar procedure, except for reducing the Ni precursor ($NiCO_3$, 98% purity, Alfa) content by 5% during the sintering step. The accurate chemical composition of LTNNO-ND was determined through inductively coupled plasma optical emission spectrometer (ICP-OES) analysis.

DFT calculation:

To investigate oxygen redox reactions, we employed the Vienna ab initio simulation package (VASP) for density functional theory (DFT) calculations using the projector augmented-wave (PAW) approach.[33,34] Crystal structures were fully relaxed using the strongly constrained and appropriately normed (SCAN) exchange-correlation functional,[35] a member of the meta-generalized gradient approximation (meta-GGA). SCAN has demonstrated superior performance compared to conventional functionals like Perdew–Burke–Ernzerhof (PBE) or PBE+U for oxide cathode materials,[36] avoiding the arbitrary selection of the U correction term. Brillouin Zone integration utilized a 3x3x3 k-mesh grid generated through the Monkhorst-Pack method. The plane-wave cut-off energy was set at 520 eV. Optimization of lattice parameters and atomic positions continued until the forces converged below 0.02 eV/Å. All calculations were spin-polarized. For an accurate calculation of the ground state electronic structure, the Heyd-Scuseria-Ernzerhof (HSE) functional was adopted to describe electron interactions,[37] with a mixing parameter of 0.25 based on previous studies.[12] Details about structure model generation can be found in Supplementary Note 1. Visualization of structures and charge densities was performed using the VESTA software.[38]

Neutron total scattering data collection and analysis

Neutron total scattering data were collected at 300 K at Spallation Neutron Source (SNS)'S NOMAD beamline of Oak Ridge National Laboratory.[39,40] Four 24 min scans (2C proton charge each) were collected and summed together for each sample to improve the statistics. Powder samples were loaded into 3mm thin-walled quartz capillaries for measurement. Background was corrected by subtracting the scattering signal from empty 3mm quartz capillary. The background subtracted scattering data were then normalized by the scattering intensity from a 6 mm vanadium rod to correct for the detector efficiency and incident neutron beam profile. The LTNNO and LTNNOF supercell models were generated using the RMCProfile Software.[41,42,43] The corresponding supercells were initially

built according to the stoichiometric ratios. During the RMC fitting procedure, the distribution and coordinates of the ions were then continuously adjusted such that the calculated neutron scattering data [including Bragg, F(Q), and G(r)] gradually approximated those observed from real neutron scattering experiments. We introduced the distance window constraints and the BVS constraints to guarantee that the supercells were kept physically rational during the adjustments.[44] To acquire random LTNNO and LTNNOF supercell models we simply shuffle the ions in the initially built supercells so that the pre-existing orders were eliminated. Details of the RMC fitting methods could be referred to in the Method section of our previous work.[9]

Electrochemical testing:

The as-prepared materials were processed through ball milling with carbon nanotubes (CNT). Following this, a composite electrode film was produced by blending the active material (70 wt%), CNT (20%), and polyvinylidene fluoride (PVDF, 10 wt%) in N-methyl pyrrolidinone (NMP) solvent. The resulting mixture was then applied onto an aluminum foil and dried overnight under vacuum conditions. For the electrochemical testing, a CR2032-type coin cell was assembled within an argon-filled glove box. The cell comprised a lithium foil as the anode, a porous polypropylene film as the separator, and a 1 M LiFP6 electrolyte dissolved in ethylene and diethyl carbonate (EC/DEC, 3:7 in volume). Galvanostatic charge and discharge tests were conducted utilizing a Land CT2001A battery test system within a voltage range of 1.5-4.8 V and at a current density of 50 mA/g, operating at a temperature of 25°C.

Author Contributions

Sichen Jiao: Conceptualization, Investigation, Formal analysis, Validation, Writing -original draft.
Yujian Sun: Formal analysis, Validation, Writing - review & editing.
Dekai Shi: Investigation, Formal analysis, Validation.
Yuanpeng Zhang: Investigation, Methodology, Formal analysis.
Jue Liu: Investigation, Resources, Writing – review & editing.
Xuelong Wang: Conceptualization, Investigation, Writing – review & editing.
Le Kang: Resources, Methodology.
Fangwei Wang: Methodology, Resources
Xiqian Yu: Conceptualization, Writing – review & editing, Funding Acquisition, Supervision.
Hong Li: Funding Acquisition, Supervision.
Liquan Chen: Funding Acquisition, Supervision.
Xuejie Huang: Funding Acquisition, Supervision.

Conflicts of interest

There are no conflicts to declare.

Acknowledgments

The work was supported by funding from the National Natural Science Foundation of China (grant nos. U1932220, 52325207, and 22239003), CAS Project for Young Scientists in Basic Research (Grant No. YSBR-058) and National Key Research and Development Program of China (No. 2021YFB2500300). This work has been partially supported by UT-Battelle, LLC, under Contract No. DE-AC05-00OR22725 with the US Department of Energy.

included in your manuscript here. Please note that this statement is required for all submitted manuscripts. If no conflicts exist, please state that "There are no conflicts to declare".

Notes and references

1 C. P. Grey and D. S. Hall, Nat. Commun., 2020, 11, 6279.
2 . Liu, Z. Bao, Y. Cui, E. J. Dufek, J. B. Goodenough, P. Khalifah, Q. Li, B. Y. Liaw, P. Liu, A. Manthiram, Y. S. Meng, V. R. Subramanian, M. F. Toney, V. V. Viswanathan, M. S. Whittingham, J. Xiao, W. Xu, J. Yang, X. Q. Yang and J. G. Zhang, Nat. Energy, 2019, 4, 180-186.
3 J. Liu, J. Wang, Y. Ni, K. Zhang, F. Cheng and J. Chen, Mater. Today, 2021, 43, 132-165.
4 S. Jiao, J. Wang, Y.-S. Hu, X. Yu and H. Li, ACS Energy Lett., 2023, 8, 3025-3037.
5 Y. Fan, W. Zhang, Y. Zhao, Z. Guo and Q. Cai, Energy Stor. Mater., 2021, 40, 51-71.
6 H. Li, R. Fong, M. Woo, H. Ahmed, D. H. Seo, R. Malik and J. Lee, Joule, 2022, 6, 53-91.
7 J. Lee, A. Urban, X. Li, D. Su, G. Hautier and G. Ceder, Science, 2014, 343, 519-522.
8 Y. Sun, S. Jiao, J. Wang, Y. Zhang, J. Liu, X. Wang, L. Kang, X. Yu, H. Li, L. Chen and X. Huang, J. Am. Chem. Soc., 2023, 145, 11717-11726.
9 S. Jiao, Y. Sun, J. Wang, D. Shi, Y. Li, X. Jiang, F. Wang, Y. Zhang, J. Liu, X. Wang, X. Yu, H. Li, L. Chen and X. Huang, Adv. Energy Mater., 2023, 13, 2301636
10 B. Li and D. Xia, Adv. Mater., 2017, 29, 1701054.
11 M. Sathiya, G. Rousse, K. Ramesha, C. P. Laisa, H. Vezin, M. T. Sougrati, M. L. Doublet, D. Foix, D. Gonbeau, W. Walker, A. S. Prakash, M. Ben Hassine, L. Dupont and J. M. Tarascon, Nat. Mater., 2013, 12, 827-835.
12 D. H. Seo, J. Lee, A. Urban, R. Malik, S. Kang and G. Ceder, Nat. Chem., 2016, 8, 692-697.
13 B. Li, N. Jiang, W. Huang, H. Yan, Y. Zuo and D. Xia, Adv. Funct. Mater., 2017, 28, 1704864.
14 R. Fukuma, M. Harada, W. Zhao, M. Sawamura, Y. Noda, M. Nakayama, M. Goto, D. Kan, Y. Shimakawa, M. Yonemura, N. Ikeda, R. Watanuki, H. L. Andersen, A. M. D'Angelo, N. Sharma, J. Park, H. R. Byon, S. Fukuyama, Z. Han, H. Fukumitsu, M. Schulz-Dobrick, K. Yamanaka, H. Yamagishi, T. Ohta and N. Yabuuchi, ACS Cent. Sci., 2022, 8, 775-794.
15 X. Li, Y. Qiao, S. Guo, Z. Xu, H. Zhu, X. Zhang, Y. Yuan, P. He, M. Ishida and H. Zhou, Adv. Mater., 2018, 30, 1705197.
16 F. Ning, B. Li, J. Song, Y. Zuo, H. Shang, Z. Zhao, Z. Yu, W. Chu, K. Zhang, G. Feng, X. Wang and D. Xia, Nat. Commun., 2020, 11, 4973.
17 J. Liu, Z. Du, X. Wang, S. Tan, X. Wu, L. Geng, B. Song, P. H. Chien, S. M. Everett and E. Hu, Energy Environ. Sci., 2021, 14, 6441-6454.
18 F. Geng, B. Hu, C. Li, C. Zhao, O. Lafon, J. Trébosc, J.-P. Amoureux, M. Shen and B. Hu, J. Mater. Chem. A, 2020, 8, 16515-16526.

19 S. Chen, S. Jiao, Q. Liang, P. Li, J. Yin, Q. Li, X. Yu, Q. Li, Anal. Chem. 2024, 96, 8021–8035.
20 E. Zhao, Q. Li, F. Meng, J. Liu, J. Wang, L. He, Z. Jiang, Q. Zhang, X. Yu, L. Gu, W. Yang, H. Li, F. Wang and X. Huang, Angew. Chem. Int. Ed. Engl., 2019, 58, 4323-4327.
21 J.H. Song, G. Yoon, B. Kim, D. Eum, H. Park, D.H. Kim, K. Kang, Adv. Energy Mater., 2020, 10, 2001207
22 Y. Li, X. Zhao, Q. Bao, M. Cui, W. Qiu, J. Liu, Energy Stor. Mater., 2020, 32, 253-260.
23 K. Zhou, S. Zheng, F. Ren, J. Wu, H. Liu, M. Luo, X. Liu, Y. Xiang, C. Zhang, W. Yang, L. He and Y. Yang, Energy Stor. Mater., 2020, 32, 234-243.
24 X. Wang, X. Fan, X. Yu, S. Bak, Z. Shadike, I. Waluyo, A. Hunt, S. D. Senanayake, H. Li, L. Chen, C. Wang, R. Xiao, E. Hu and X. Q. Yang, Adv. Funct. Mater., 2020, 31, 2001633.
25 R. A. House, U. Maitra, L. Jin, J. G. Lozano, J. W. Somerville, N. H. Rees, A. J. Naylor, L. C. Duda, F. Massel, A. V. Chadwick, S. Ramos, D. M. Pickup, D. E. McNally, X. Lu, T. Schmitt, M. R. Roberts and P. G. Bruce, Chem. Mater., 2019, 31, 3293-3300.
26 M. M. Rahman and F. Lin, Matter, 2021, 4, 490-527.
27 B. Li, K. Kumar, I. Roy, A. V. Morozov, O. V. Emelyanova, L. Zhang, T. Koc, S. Belin, J. Cabana, R. Dedryvere, A. M. Abakumov and J. M. Tarascon, Nat. Mater., 2022, 21, 1165-1174.
28 M. D. Radin, J. Vinckeviciute, R. Seshadri and A. Van der Ven, Nat. Energy, 2019, 4, 639-646.
29 D. Chen, W. H. Kan and G. Chen, Adv. Energy Mater., 2019, 9, 1901255.
30 A. Outka, H. Ho, W.C.H. Kuo, Y. Wang, B. Raji-Adefila, S. Sainio, D. Nordlund, J. Watt, J.H., Wang, D. Chen, ACS Energy Lett., 2024, 9, 1863-1870.
31 E. Lee, D.H. Lee, S. Bessette, S.W. Park, N. Brodusch, G. Lazaris, H. Kim, R. Malik, R. Gauvin, D.H. Seo, J. Lee, Energy Environ. Sci., 2024. DOI: 10.1039/d4ee00551a
32 E. Zhao, L. He, B. Wang, X. Li, J. Zhang, Y. Wu, J. Chen, S. Zhang, T. Liang, Y. Chen, X. Yu, H. Li, L. Chen, X. Huang, H. Chen and F. Wang, Energy Stor. Mater., 2019, 16, 354-363.
33 G. Kresse and J. Furthmüller, Comput. Mater. Sci., 1996, 6, 15-50.
34 P. E. Blochl, Phys. Rev. B Condens. Matter, 1994, 50, 17953-17979.
35 J. Sun, A. Ruzsinszky and J. P. Perdew, Phys. Rev. Lett., 2015, 115, 036402.
36 A. Chakraborty, M. Dixit, D. Aurbach and D. T. Major, npj Comput. Mater., 2018, 4.
37 J. Heyd, G. E. Scuseria and M. Ernzerhof, J. Chem. Phys., 2003, 118, 8207-8215.
38 K. Momma and F. Izumi, J. Appl. Crystallogr., 2011, 44, 1272-1276.
39 S. Calder, K. An, R. Boehler, C. R. Dela Cruz, M. D. Frontzek, M. Guthrie, B. Haberl, A. Huq, S. A. J. Kimber, J. Liu, J. J. Molaison, J. Neuefeind, K. Page, A. M. Dos Santos, K. M. Taddei, C. Tulk and M. G. Tucker, Rev. Sci. Instrum., 2018, 89, 092701.
40 J. Neuefeind, M. Feygenson, J. Carruth, R. Hoffmann and K. K. Chipley, Phys. Res. B, 2012, 287, 68-75.
41 G. Evrard and L. Pusztai, J. Phys. Condens. Matter, 2005, 17.
42 M. G. Tucker, D. A. Keen, M. T. Dove, A. L. Goodwin and Q. Hui, J. Phys. Condens. Matter, 2007, 19, 335218.
43 Y. Zhang, M. Eremenko, V. Krayzman, M. G. Tucker and I. Levin, J. Appl. Crystallogr., 2020, 53, 1509–1518.
44 S. T. Norberg, M. G. Tucker and S. Hull, J. Appl. Crystallogr., 2009, 42, 179–184.